Title

Design and Evaluation of a Multispectral Imaging Device for Cerebral Oxygenation Measurements

Permalink

https://escholarship.org/uc/item/6mf7g8bg

Author

Dhariwal, Guriqbal Singh

Publication Date

2018

Peer reviewed|Thesis/dissertation

UNIVERSITY OF CALIFORNIA,

IRVINE

Design and Evaluation of a Multispectral Imaging Device for Cerebral Oxygenation

Measurements

THESIS

Submitted in partial satisfaction of the requirements for the degree of

MASTER OF SCIENCE

in Biomedical Engineering

by

Guriqbal Dhariwal

Thesis Committee:
Professor Bernard Choi, Chair
Professor Bruce J. Tromberg
Professor Michelle Digman

2018

Dedication

Dedicated to friends and family who have stood by me through thick and thin.

Table of Contents

List of Figures

List of Tables

Abstract

By

Guriqbal Dhariwal

Master of Science in Biomedical Engineering

University of California, Irvine, 2018

Professor Bernard Choi, Chair

Knowledge of cerebral oxygenation is critical to an understanding of brain status in normal physiology and especially in development of pathophysiological conditions, such as cerebral amyloid angiopathy. This thesis describes development and evaluation of a simple multispectral reflectance imaging device. The device was modeled after a previously published paper by Dunn et al., and consists of a 3-D printed filter wheel, a CCD camera, a motor driving circuit, a photodiode, an Arduino, a light source and six bandpass filters. Two approaches to calculate differential pathlength factor (DPF) values were investigated and compared with published values from Dunn et al., and a surprising finding was that a DPF algorithm derived originally for point spectroscopy was the most accurate approach of the three to calculate changes in oxy- and deoxyhemoglobin. Further studies are warranted.

Chapter 1: Introduction to CAA & Reflectance Imaging

1.1 Background:

Cerebral amyloid angiopathy(CAA) causes β-amyloid protein to deposit in the middle and outermost layer of arteries in the brain. This in turn can lead to dementia, intracranial hemorrhage, or ischemic infarcts. CAA is a hallmark of Alzheimer's disease but is also found in healthy elderly people. (1) A study done in 1987 of 123 brain autopsies showed that 57% of the brains (ages 59-101 years) had CAA. (2) The damage done by CAA can leave individuals debilitated. For example, only 20% of individuals who experience intracranial hemorrhages become independent after 6 months. (3)

This thesis describes the creation of a visible light reflectance spectroscopy imaging system, that can be used to study the effects of CAA on the brain. Using visible light reflectance spectroscopy, the progression of CAA can be explored with transgenic mouse models of human CAA. By nine months of age, these mice have elevated levels of β-amyloid . (4) As the β-amyloid protein deposits form, CAA reduces vascular reactivity which in turn can reduce perfusion. This may mean that when the brain performs tasks that requires oxygenated hemoglobin (HbO2) in one area, the lack of perfusion may reduce the oxygenated hemoglobin and cause ischemic damage. (5) It has also been shown that healthy elderly subjects have a greater change in HbO2 concentration than elderly subjects with Alzheimer's disease. (6)

The peptide Amyloid Protein Precursor (APP) when cleaved by β -secretase and Y-secretase leads to the formation of the β-amyloid protein. In the presence of β -secretase inhibitor the β-amyloid protein is prevented from being formed. (7) With this knowledge, experiments can be performed with the use of visible light reflectance spectroscopy to study the effects of β -secretase inhibitor, as well as other therapeutic approaches. The relative HbO2 and deoxygenated (HbO) hemoglobin (Hb) concentrations of mice with CAA and no inhibitor can be measured and be compared to the relative concentrations of mice with CAA and the inhibitor.

In addition, this thesis describes the traditional method to calculate the relative HbO2 and HbO concentrations (ΔCi) using the modified Beer-Lambert Law (equation 1).

$$A(\lambda)=\sum \epsilon i(\lambda)\Delta Ci\, DPF(\lambda) \tag{1}$$

The term $\epsilon i(\lambda)$ represents the extinction coefficient of the chromophore of interest, $\Delta A(\lambda)$ represents the change in absorbance of light caused by the chromophore, and $DPF(\lambda)$ represents the differential pathlength factor, which is a number that scales with the mean optical pathlength that photons travel in tissue. (8)

This thesis will describe a different approach to calculating the differential path length factor (DPF) to use in conjunction with this system. Traditionally DPF values are calculated using the equation 2. (8)

$$\partial A(\lambda)/\partial \mu a(\lambda) \tag{2}$$

 It was discovered more accurate DPF values can be calculated using the following equation:

$$\frac{1}{2}\left(\frac{3\mu_s'(\lambda)}{\mu_a(\lambda)}\right)^{1/2} \tag{3}$$

Equation 3 was originally used to calculate DPF values for a Continuous Wave – Near Infrared (CW-NIR) spectroscopy system. It was found when the DPF values from equation 2 were used to solve equation 1, the relative HbO2 and HbO concentrations were more accurate. (9)

1.2 What is Absorbance Spectroscopy?

Absorbance spectroscopy takes advantage of the light absorbing properties of a substance and uses the Beer-Lambert Law to calculate the concentration of the substance. The Beer-Lambert Law is the relationship A = e*l*C where A is absorbance, e is the extinction coefficient, and C is the concentration. A is a measure of how much light has been absorbed, the extinction coefficient is a measure of how well a molecule absorbs a particular wavelength of light, and l is the pathlength that the light travels. Using a modified version of this relationship, the

concentrations of HbO2 and HbO can be calculated. (10) Figure 1 shows light traveling straight through a substance in a cuvette. Absorbance is calculated using log10(I0/I), where I0 is the light intensity before it passes through the sample and I is the light intensity after it passes through the sample. Knowing the absorbance, the path length the light travels, and the extinction coefficient, the concentration c of the substance in the cuvette can be calculated. (11)
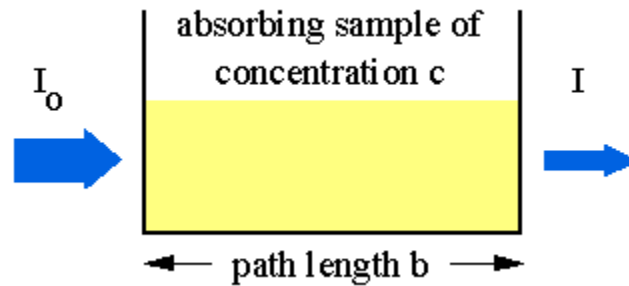
Figure 1: Cuvette of some pathelength b with light passing through it (11)

1.3 What is reflectance spectroscopy?

Reflectance spectroscopy involves illuminating light onto tissue and measuring the reflectance intensities at different timepoints. The reflectance intensity is the light that is scattered back to the detector(camera) from the tissue. By knowing the reflectance intensities of the tissue at one timepoint and a later timepoint, the modified Beer-Lambert Law can be used to calculate the change in concentration of a chromophore of interest.

To calculate relative hemoglobin concentration, the modified Beer- Lambert Law must be used (Equation 1). The modified Beer- Lambert Law replaces the concentration term in the Beer-Lambert Law with ΔC_i , the absorbance term with ΔA and the pathlength term with differential pathlength factor($DPF(\lambda)$. Differential pathlength is defined as $\partial A(\lambda)/\partial \mu a(\lambda)$ and scales with the mean optical pathlength that photons travel in tissue.

The visible reflectance spectroscopy device illuminates light on an object and the intensity of the light coming back from it is measured at two different time points (t1 = 0(s) and t2 = X(s)). The change in absorbance (ΔA) is then quantified by log(I0(t1)/I(t2)). (8) The extinction coefficient($\epsilon i(\lambda)$) for HbO2 and HbO can be found in literature. The differential pathlength($DPF(\lambda)$) can be calculated by the equation $\partial A(\lambda)/\partial \mu a(\lambda)$, $\partial A(\lambda)$ is a small change in absorption at a particular wavelength and $\partial \mu a(\lambda)$ is a small change in the absorption coefficient at a particular wavelength. (8) In order to use equation 2, first the μa values are calculated for each wavelength and are perturbed. Secondly, the corresponding absorption values are calculated for each perturbed μa value. Lastly, $A(\lambda)$ values versus μa(λ) values are plotted for each wavelength and a line is then fit to the data so the slope of the line is then equal to the DPF value.

Furthermore, each wavelength of light when illuminated on the tissue gets absorbed by both HbO2 and HbO. Thus, equation 1 can be rewritten as equation 4.

$\Delta A(\lambda)$ = $\epsilon oxy(\lambda)\Delta CoxyDa(\lambda)$ + $\epsilon deoxy(\lambda)\Delta CdeoxyDa(\lambda)$.   (4)

Since there are 6 wavelengths, there are 6 equations that can be used to solve for $\Delta Coxy$ and $\Delta Cdeoxy$. The 6 equations can be rewritten in matrix form and $\Delta Coxy$ and ΔCdeoxy can be solved for by performing a simple linear regression.

$$
\begin{bmatrix} \Delta A(560) \\ \Delta A(570) \\ \Delta A(580) \\ \Delta A(590) \\ \Delta A(600) \\ \Delta A(610) \end{bmatrix} = \begin{bmatrix} \epsilon_{oxy}(560)DPF(560) & \epsilon_{deoxy}(560)DPF(560) \\ \epsilon_{oxy}(570)DPF(570) & \epsilon_{deoxy}(570)DPF(570) \\ \epsilon_{oxy}(580)DPF(580) & \epsilon_{deoxy}(580)DPF(580) \\ \epsilon_{oxy}(590)DPF(590) & \epsilon_{deoxy}(590)DPF(590) \\ \epsilon_{oxy}(600)DPF(600) & \epsilon_{deoxy}(600)DPF(600) \\ \epsilon_{oxy}(610)DPF(610) & \epsilon_{deoxy}(610)DPF(610) \end{bmatrix} * \begin{bmatrix} \Delta C_{oxy} \\ \Delta C_{deoxy} \end{bmatrix}
$$ (Matrix 1)

Chapter 2: Device Design

2.1 Overview of Device:

In order, to create a visible light reflectance spectroscopy system, a 3d printed filter wheel, a CCD camera, a motor driving circuit, a photodiode, an Arduino micro-computer and a white light source were used. The filter wheel consists of a 560 nm filter, a 570 nm filter, a 580 nm filter, a 590 nm filter, a 600 nm filter, and a 610 nm filter. The filter wheel is attached to the motor and the motor is driven by a motor driving circuit. The speed of the motor is controlled with an Arduino. A photodiode along with a laser pointer are used to trigger the camera, to keep track of the position and to keep track of the speed of the motor. Figure 2 shows a picture of the device.
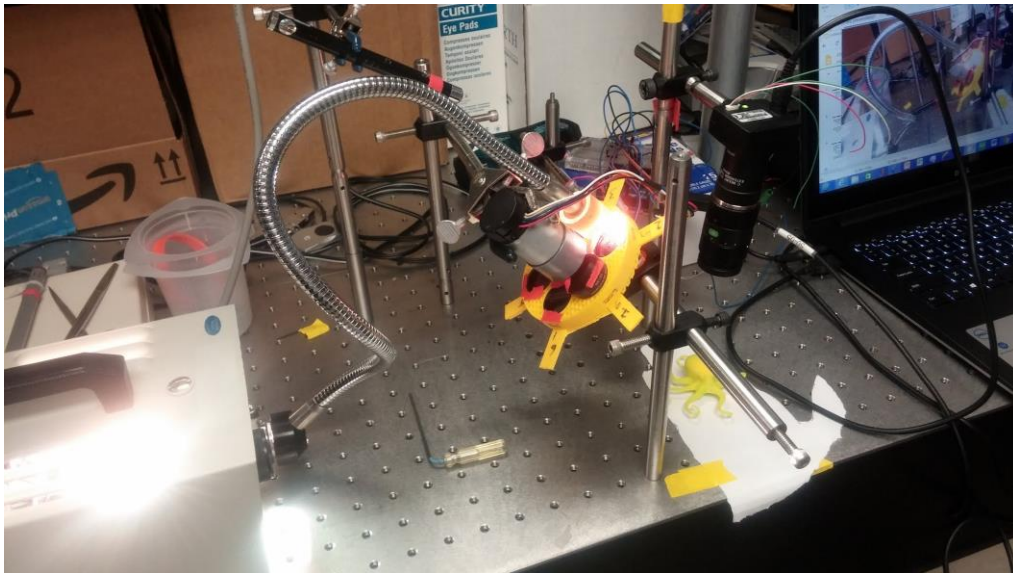
Figure 2: Visible Light Reflectance Spectroscopy Device

2.2 Motor Driving Circuit:

The motor driving circuit consists of a 25 kOhm resistor, a TIP120 transistor, a 12 volt sainsmart 29:1 Metal Gearmotor, a diode (this allows current to travel only one way to protect the motor), and an Arduino. Figure 2 shows the motor driving circuit.
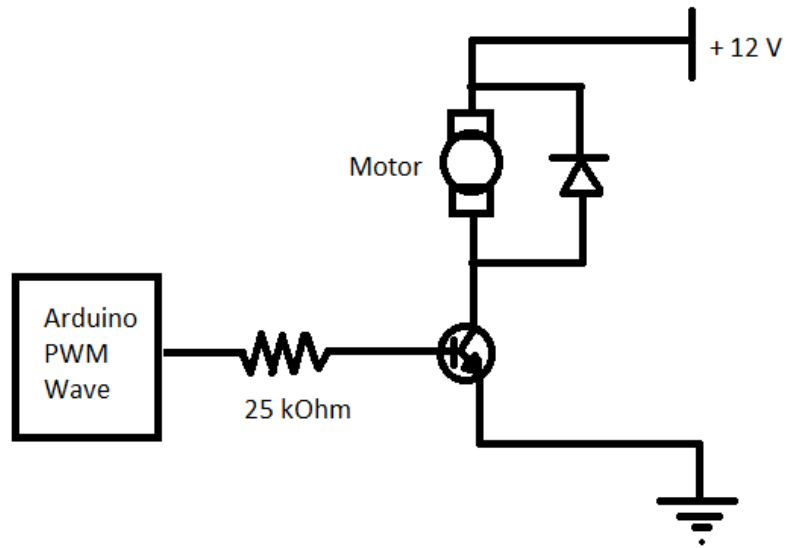
Figure 3: The motor driving circuit

The transistor helps to control the speed of the motor. A pulse modulated wave from the Arduino is sent into the base of the transistor. The pulse modulated wave is a square shape wave that alternates between 5 volts and 0 volts. This wave when sent into the base of the transistor, turns it on and off. To increase the speed of the motor, the duration the switch is on must be increased. This is done by increasing the duty cycle (making the pulse wider) of the pulse modulated wave. (12) An example of a pulse modulated wave can be seen in figure 4.
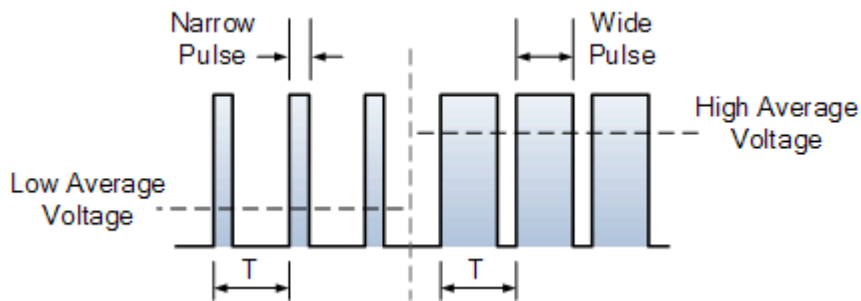
Figure 4: PWM Wave. The narrower the pulse, the slower the motor. The Wider pulse, the faster the motor (13)

6

The width of the PWM is changed with the following piece of Arduino code

```
if(increment4 == 0){    //setupposition function is only used once in this program

    Serial.println("Enter value from 0 to 255"); // tells user to enter value from 0 to 255
    delay(5000); //Gives user 5 seconds to enter a value
    increment4 = 1;
  }
  if (Serial.available())
  {
   int speed = Serial.parseInt();//
  }
```

This piece of code prompts the user to input a value from 0 to 255. The higher the input value is,

the greater the width/duty cycle of the PWM, and thus greater the speed of the motor. The

reason a 25 kOhm resistor is used in the circuit is to make sure that the motor does not receive

more than 200 mA of current when the PWM is in its high state (5 volts). Anything more than

200 mA can cause the motor to break. Knowing that the current input into the base of the

TIP120 transistor is amplified by a gain of 1000, it was calculated that the maximum current that

can be input into the base must be no more than .2 mA. The PWM voltage that is input into the

base of the transistor has a high of 5 V, so using V = IR it was then calculated that the base

resistor value must be 25 kOhms. (12)

2.3 Position, RPM, and Camera Triggering for Device:

One important aspect of the device is knowing how fast the motor is spinning. By knowing how

fast the motor is spinning, the speed can be adjusted to the user's needs. The RPM of the motor

is measured using the built-in encoder of the motor which outputs approximately 962 high and

low pulses every revolution to the Arduino. The Arduino is programmed to store the number of

pulses every 0.25 seconds. The number of pulses in 0.25 seconds is divided by the total

number of pulses (962) multiplied by 0.25 seconds to obtain the number of revolutions per

second. This number is then converted to revolutions per minute. The Arduino program to do

this can be seen below.

```
void RPMofMotor(){
 if(millis() - start > fin){// if millis() is greater than .24 enter
this statement
  noInterrupts();  //don't allow program to interrupt until the
following is comeplte
  rpm = (pulse*60)/(960*.25); // Calculates RPS and convert to RPM by
multiply by 60
  Serial.println(rpm) //Print RPM's onto serial screen
  pulse = 0; //reset pulses to 0
  start = millis(); //restart timer
  interrupts(); // allow program to interrupt
  }
}

void readEncoder()
{
  ++pulse;
}
```

In order, to check whether this method of calculating RPM's was correct, the RPM of the motor

at different voltages were first measured using the encoder (figure 6) and a power supply. The

speed of the motor was modulated by varying the voltage (1 to 12 volts) that the power supply

sent to the motor. The RPM's measured using an encoder were compared to the RPM's

calculated using a OPT101PG4 photodiode and a light source. A q-tip attached to the shaft of

the motor, and a light source was used to illuminate the photodiode (figure 5).

Whenever the light source would be interrupted by the q-tip, it meant that one revolution had
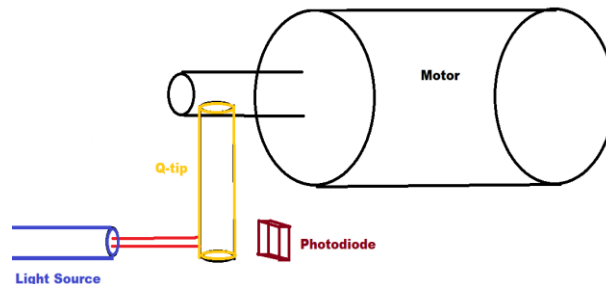
Figure 5: Motor interrupting light source RPM experiment setup

happened. The time it took for a revolution to happen was used to calculate revolutions per

minute. As can be seen from the photodiode vs encoder RPM graph, the slope of the fitted

model is approximately 1 meaning that the photodiode and encoder give approximately the

same RPM values (figure 6). The RPM vs voltage is plotted in figure 7.
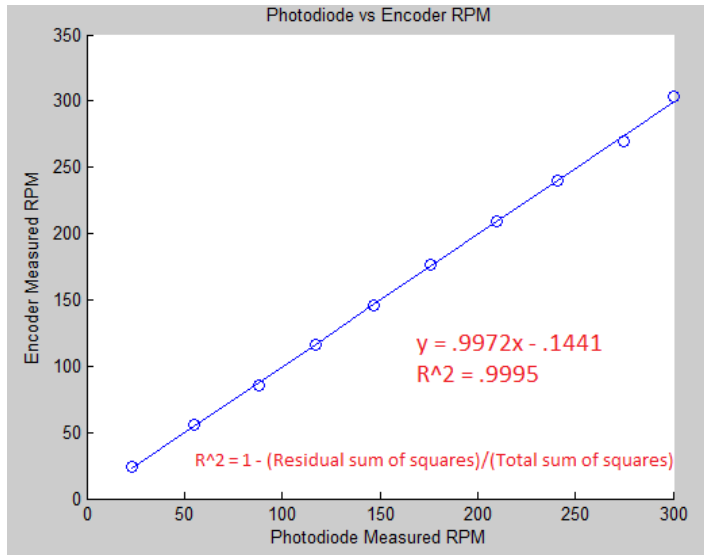
Figure 6: Photodiode RPM plotted against Encoder RPM values
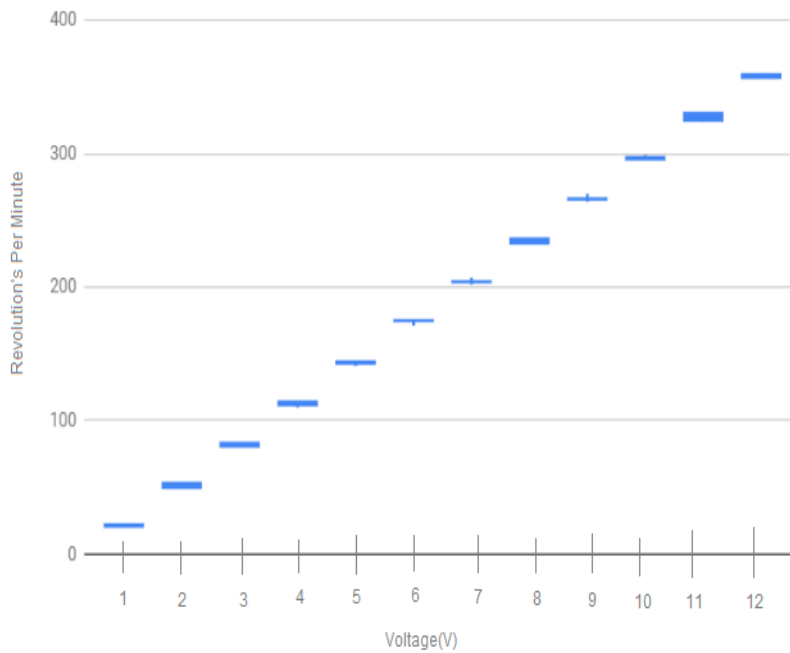
Figure 7: Box Whisker Plot of RPM vs Voltage(v) measured using a photodiode
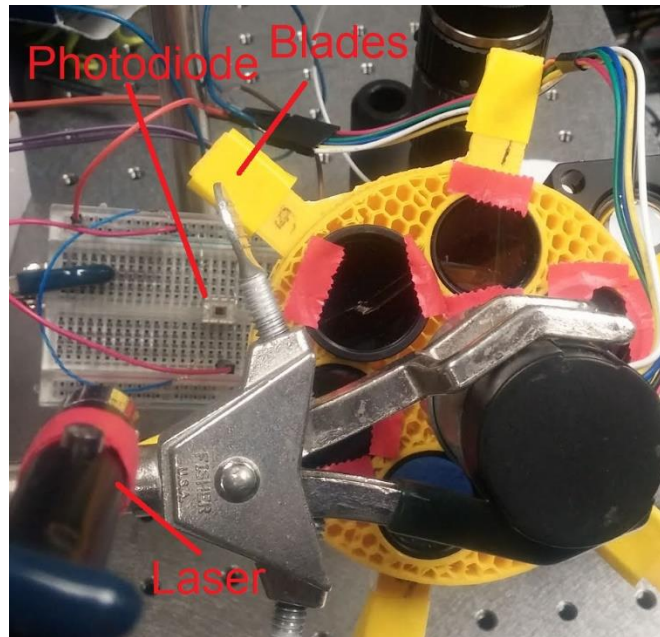
Figure 8: Blades of the filter wheel labeled, block the laser preventing light from getting to the photodiode

Another important aspect of this device is to determine which filter is being used each time the

camera snaps an image. Each filter is located next to a blade that is labeled with a position

number from 1 to 6 counterclockwise. In order, to keep track of which position the filter wheel is

on, a photodiode, a laser, and an Arduino were used (figure 7). An Arduino program was

written to display the position number on the computer screen.

```
sensorvalue = analogRead(sensorPin);

//  Serial.println(sensorvalue);

    if (increment2 == 1){ //Can not continue past this point unless the

senorvalue is >= 800

    if(sensorvalue < 710){// If the sensor value falls below 710
      if(position1 == 6){ // if the last position of the filter wheel was 6,
set the new position to zero
        position1 = 0;
      }
    digitalWrite (pin, LOW); // set camera pin to Low, this will trigger the
camera
    position1 = position1 + 1; // add 1 to the position value

    Serial.println(position1);Serial.print("\t");
    increment3 = 1;
    increment2 = 0;
    }
  }
```

```
  if(increment3 == 1){
     if(sensorvalue >= 800){
        digitalWrite (pin, HIGH);
      increment2 = 1;
      increment3 = 0;
     }
  }
    sensorvalue2 = sensorvalue;
}
```

The program displays the position at which each image is taken by determining if one of the

blades has passed over the photodiode. A laser is pointed at the photodiode, such that when

the photodiode's sensor value is read by the Arudino, the intensity is 800 or greater. When the

motor spins and one blade of the filter wheel covers the photodiode, the intensity value

decreases below a count of 710. When the Arduino program starts and before the filter wheel

starts spinning it tells the user to input the last number of the last filter wheel blade that had

passed the photodiode counterclockwise. Once this position has been input, the Arduino starts

to read in the sensor value from the photodiode. After the motor starts spinning and the

photodiode is covered temporarily by one of the blades of the filter wheel, the sensor value will

decrease below 710. When this happens, the Arduino is programmed to display the previous

position incremented by 1. If the last position is 6 and a blade covers the photodiode, then the

Arduino will display a 1 on the computer screen. In addition, the Arduino sends a low signal to

the camera when it increments the position by 1, which triggers the camera to take an image.

Chapter 3: DPF Calculations and Testing

3.1 Calculating DPF values/Concentrations:

In order, to calculate the DPF values using equation 2, the μ_a values were first calculated using

equations 5, 6, 7, and 8 that were found in a paper published by Jacques et al. (14)

$$\mu_a = BS\mu_{a,oxy} + B(1-S)\mu_{a,deoxy} + W\mu_{a,water} + F\mu_{a,fat} + M\mu_{a,melanosome} + 2.3C_{bili}\varepsilon_{bili} + 2.3C_{\beta C}\varepsilon_{\beta C} \quad (5)$$

$$B = CHGB/tHb \quad (6)$$

$$\mu_{a,oxy} = 2.303 * \epsilon_{oxy}(\lambda) * tHb \quad (7)$$

$$\mu_{a,deoxy} = 2.303 * \epsilon_{deoxy}(\lambda) * tHb \quad (8)$$

B is blood volume fraction, S is oxygen saturation, $\mu_{a,oxy}$ is the absorption coefficient of HbO2 in

whole blood, $\mu_{a,deoxy}$ is the absorption coefficient of HbO in whole blood, CHGB is the total

hemoglobin concentration of the rat brain cortex, tHb is the total hemoglobin concentration of

whole blood. Different values were found for CHGB and S, so the average of each was taken.

(14)

Table 1: CHGB, S, tHb constants (14)

CHGB	(87.3 + 71.0)/2 = 79.15 uM
S	(60.7 + 59.0)/2 = 59.85 %
tHb	(150 g/liter)/(64,500 g Hb/mole) = .00233 M

The terms involving water, fat, bilirubin(denoted bili in Eq. (5)), and β -carotene(denoted βC in

Eq. (5)) were assumed to be negligent. The terms for melanin, which is not relevant for brain

tissue, were also set to zero. μ_s' for each wavelength is calculated using the following equation:

$$\mu_s'(\lambda) = a'(f_{ray}\left(\frac{\lambda}{500\ (nm)}\right)^{-4} + (1 - f_{ray})\left(\frac{\lambda}{500\ (nm)}\right)^{-b_{Mie}} \tag{9}$$

$$\mu_s(\lambda) = \frac{\mu_s'(\lambda)}{(1-g)} \tag{10}$$

The first part of the equation $a'(f_{ray}\left(\frac{\lambda}{500\ (nm)}\right)^{-4}$ describes Rayleigh scattering, and the second

part $(1 - f_{ray})\left(\frac{\lambda}{500\ (nm)}\right)^{-b_{Mie}}$ describes Mie scattering. f_{ray} represents the fraction of Rayleigh

scattering, $(1 - f_{ray})$ represents the fraction of Mie scattering, b_{Mie} represents the scattering

power of Mie scattering, and λ represents the wavelength of light. (14)

Table 2: Table used to calculate μ_s' (14)

a'	27.4 (cm^-1)
f_{ray}	.315
b_{Mie}	1.087
g	.9

After calculating μ$_a$ for the 6 wavelengths, we then calculated μ$_a$ values that were 90%, 95%,

105%, and 110% of each μ_a value. This was done to enable estimation of ∂A(λ)/∂μa(λ) at each

of the six wavelengths, by performing a linear regression of A versus μ$_a$.

Table 3: μ_a values for rat brain cortex at wavelengths 560, 570, 580, 590, 600, 610 solved

using equation (5-8) and table 1

	560 nm	570 nm	580 nm	590 nm	600 nm	610 nm
μ_a (mm^-1)	0.7494	0.8153	0.8176	0.3644	0.1423	0.0855

Table 4: μ'_s values for rat brain cortex at wavelengths 560, 570, 580, 590, 600, 610, found using equation 9 and table 2

	560 nm	570 nm	580 nm	590 nm	600 nm	610 nm
μ'_s (mm^-1)	2.207878	2.138766	2.073941	2.013031	1.955702	1.901659

Table 5: Perturbation μ_a values of Table 2

	560 nm	570 nm	580 nm	590 nm	600 nm	610 nm
90% of Ua	0.6751	0.7344	0.7364	0.3283	0.1282	0.0771
95% of Ua	0.7126	0.7752	0.7774	0.3465	0.1353	0.0813
100% of Ua	0.7876	0.8568	0.8592	0.3830	0.1496	0.0899
105% of Ua	0.8251	0.8976	0.9001	0.4012	0.1567	0.0942

We calculated optical properties using the equations 11-17 (below) from Cuccia et al. (15)

These equations enable calculation of absorbance by subtracting the diffuse reflectance (R_d) from 1. μ_{tr} below represents the transport coefficient, A is the proportionality constant, R_{eff} is the effective reflection coefficient, and a' is the reduced albedo. The results of the absorbance values using the Cuccia equations can be seen in table 6. The results for what the absorbance values would be if they were calculated with MCS, can be seen in table 7.

$$\mu_{tr} = \mu'_s + \mu_a \tag{11}$$

$$\mu_{eff} = \sqrt{3 * \mu_a * \mu_{tr}} \tag{12}$$

$$A = \frac{1 - R_{eff}}{2(1 + R_{eff})} \tag{13}$$

$$R_{eff} \approx .0636n + .668 + \frac{.710}{n} - \frac{1.440}{n^2} \tag{14}$$

$$R_d(k) = \frac{3Aa'}{\left(\frac{\mu'_{eff}}{\mu_{tr}} + 1\right)\left(\frac{\mu'_{eff}}{\mu_{tr}} + 3A\right)} \tag{15}$$

Table 6: Absorbance values found for rat brain cortex using Table 3, 4 and Cuccia Equations

	560	570	580	590	600	610
A at 90%	0.8520	0.8630	0.8660	0.7831	0.6599	0.5884
A at 95%	0.8572	0.8679	0.8709	0.7896	0.6678	0.5966
A at 105%	0.8664	0.8767	0.8795	0.8014	0.6821	0.6115
A at 110%	0.8706	0.8806	0.8834	0.8067	0.6889	0.6185

Table 7: Absorbance values found for the rat brain cortex Table 3, 4, equation 10 and MCS

	560	570	580	590	600	610
A at 90%	.8600	.8703	.8732	.7826	.6430	.5643
A at 95%	.8635	.8766	.8790	.7879	.6518	.5741
A at 105%	.8739	.8843	.8871	.8009	.6666	.5904
A at 110%	.8769	.8887	.8920	.8068	.6757	.5962

Table 7 shows what the results of the absorbance values would be using Monte Carlo simulations (MCS) that simulate gray matter using μ_a values (table 3) and μ_s values (found using table 4 and equation 10). The monte carlo simulations used, simulate what happens when photons enter a 100 mm thick gray matter slab. The 100 mm gray matter slab is simulated in MATLAB by taking into account the absorption coefficient, scattering coefficient and its anisotropy. The photons interacting with the gray matter would either be reflected or absorbed by the tissue. At the end of a simulation the percent of photons absorbed from the total photons launched at the tissue can be seen.

MCS were used to test the accuracy of the Cuccia equations for absorbance. Table 8 shows the percent error of the absorbance values calculated with the Cuccia equations from the MCS absorbance values. It is apparent that the absorbance values from the Cuccia paper are very close to the absorbance values from the MCS.

Table 8: Percent error between the MCS and Cuccia Equations

	560	570	580	590	600	610
A at 90%	0.93%	0.84%	0.82%	0.06%	2.63%	4.27%
A at 95%	0.73%	0.99%	0.92%	0.22%	2.45%	3.91%
A at 105%	0.86%	0.86%	0.86%	0.06%	2.32%	3.57%
A at 110%	0.72%	0.91%	0.96%	0.01 %	1.95%	3.74%

Absorbance (90%, 95%,105%, 110%)(table 6) and μ_a(90%, 95%,105%, 110%)(table 5) were

plotted against each other for each wavelength; the slope of the graphs by definition is the DPF

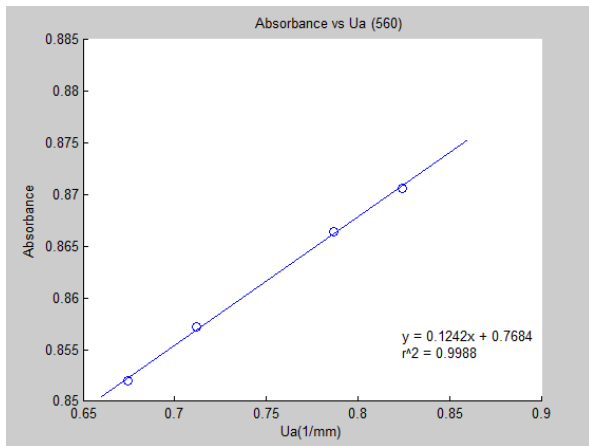value for that particular wavelength (figure 9 – 14).

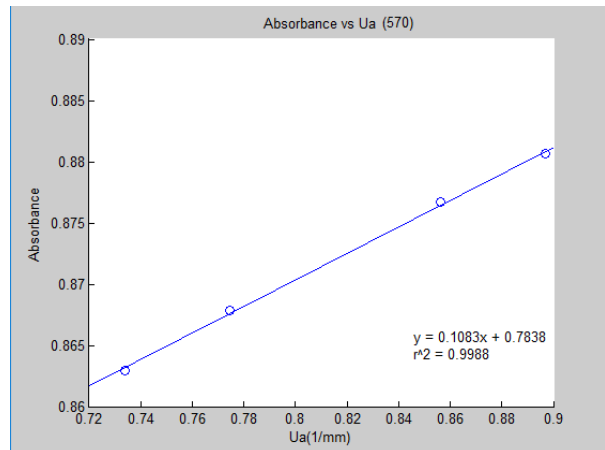*Figure 9: DPF value (slope) for 560 is .1242 mm*

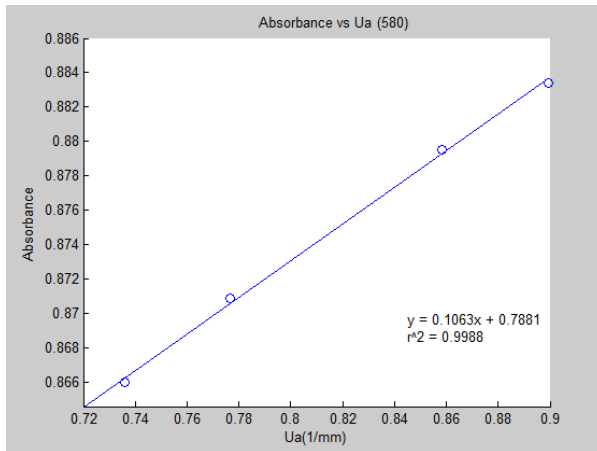*Figure 10: DPF value (slope) for 570 is .1083 mm*

Figure 11: DPF value (slope) for 580 is .1063 mm
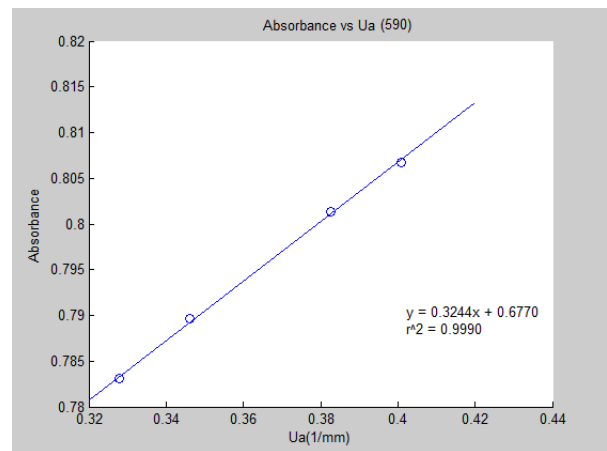

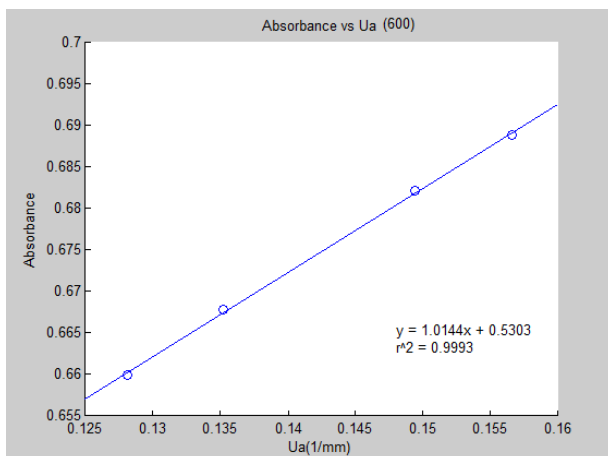*Figure 12: DPF value (slope) for 590 is .3244 mm*

Figure13: DPF value (slope) for 600 is 1.0144 mm
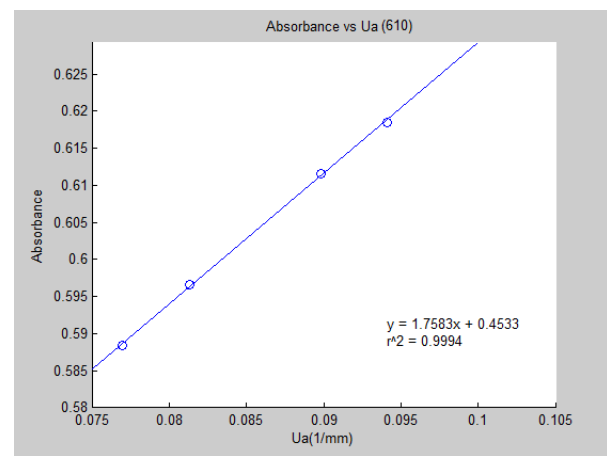
Figure 14: DPF value (slope) for 610 is 1.7583 mm

17

Table 9: Calculated DPF values calculated with CHGB = 79.15 uM and S = .5985

	560	570	580	590	600	610
$\partial A(\lambda)/\partial \mu a(\lambda)$ Calculated DPF(mm)	0.1242	0.1083	0.1063	0.3244	1.0144	1.7583

The values in Table 9 are similar to the DPF values found for a similar visible light reflectance

spectroscopy device reported on by Dunn et al. (16) The method they used to calculate the

DPF values also involves equation 2 but rather than use equation 5 to calculate the μ_a values,

they used equation 16. In addition, they assumed μ_s to be 100 cm^-1 for all wavelengths and

the values of CHGB and S that were used to calculate the baseline μ_a values, were 100 uM

and .6 respectively. (16)

$$\mu_a (\lambda) = \epsilon_{HbO2}(\lambda)Co_{HbO2}(\lambda) \quad + \quad \epsilon_{HbO}(\lambda)Co_{HbO}(\lambda) \tag{16}$$

Table 10: Dunn DPF values calculated with CHGB = 100 uM and S = .6

	560	570	580	590	600	610
Dunn DPF Values(Baseline: CHGB = 100 uM, S = .6)	.505	.5	.5	.9	1.6	2.05

These DPF values when plugged into matrix 1 allow the matrix to be solved. In addition, to

calculating the DPF values using equation 2, they were also calculated using equation 3

$(\frac{1}{2}\left(\frac{3\mu'_s(\lambda)}{\mu_a(\lambda)}\right)^{1/2})$. Equation 3 is a general equation for DPF for the frontal human head.

This equation is from a paper written by Scholkmann and Wolf (9) and the equation is meant to

be used for a CW-INR spectroscopy device. Equation 3 was used to calculate DPF values for

this visible light reflectance spectroscopy device and helped achieve better results for the

relative HbO2 and HbO concentrations than the Dunn DPF values and the $\partial A(\lambda)/\partial \mu a(\lambda)$ DPF values. Tables 3 and 4 were used along with equation 3 to solve for the DPF values in table 11.

Table 11: Scholkmann DPF values calculated with CHGB = 79.15 uM and S = .5985

	560	570	580	590	600	610
Scholkmann DPF(mm)	1.4858	1.4021	1.3787	2.0346	3.2083	4.0819

3.2 Testing of the DPF values

The 3 sets of DPF values were used in 2 experiments to see which set of values allow matrix 1 when solved, to give the most accurate relative HbO2 and HbO concentrations. The ΔA values for matrix 1 were calculated by looking at how much light would be reflected from a brain, whose initial CHGB is 79.15 uM and S is .5985, using equations 8,9,10,11, and 12. The experiments that were performed are listed below and the procedure to the experiments are listed below as well.

Experiment 1: Assuming a rat brain has an initial CHGB of 79.15 uM and an oxygen saturation of 59.85%, the initial oxygen saturation was reduced by 10%, 20%, 30%,40%, and 50%. Each time the oxygen saturation was reduced the change in concentration for HbO2 and HbO was calculated by solving matrix 1. Matrix 1 was solved 3 times, once with each set of the DPF values (table 9,10, 11). After solving for the Hb concentrations, with each set of the DPF values, they were compared to the theoretical Hb concentrations.

Experiment 2: Assuming a rat brain has an initial CHGB of 79.15 uM and an oxygen saturation of 59.85%, the initial total hemoglobin concentration of the tissue was reduced by 10 uM, 20 uM, 30 uM, 40 uM, 50 uM, 60 uM, and 70 uM. Each time the total hemoglobin concentration was reduced, the change in concentration for HbO2 and HbO was calculated by solving matrix 1. Matrix 1 was solved 3 times, once with each set of the DPF values (table 9,10,11). After solving

for the Hb concentrations, with each set of the DPF values, they were compared to the

theoretical Hb concentrations.

Experiment Concentration Calculation Procedure:

1. Calculate theoretical Changes in HbO2 and HbO for the experiments listed below

    a. Calculate theoretical initial hemoglobin concentrations using CHGB and S found

    in table 1 using the following equations

$$Initial\ HbO2\ Concentration\ =\ CHGB * S \qquad\qquad (17)$$

$$Initial\ HbO\ Concentration\ =\ CHGB * (1 - S) \qquad\qquad (18)$$

    b. Calculate theoretical final hemoglobin concentrations by modifying either CHGB

    or S using equations(17,18) (see experiments to see how much to modify CHGB

    and S by)

    c. Subtract theoretical final hemoglobin concentrations with theoretical initial

    hemoglobin concentrations to get change in theoretical HbO2 and HbO

    concentrations

    d. Repeat steps 1b to 1c until the concentrations for each change in CHGB and S is

    calculated

2. Calculate experimental changes in HbO2 and HbO using the 3 sets of DPF values

    a. Calculate the baseline μ_a (equation 5) values for each of the wavelengths using

    the CHGB and S values used for step 1a

        i. Calculate the reflectance value for each μ_a, using equations 16. Place

        the reflectance values into a vector called I0.

    b. Calculate μ_a for each of the wavelengths for a change in CHGB or S values

        i. Calculate the reflectance value for each μ_a, using equations 16. Place

        the reflectance values into a vector called I.

c. Calculate the ∆A vector(b vector) for matrix 1 by solving log10(I0/I) in MATLAB

d. Solve matrix 1 in MATLAB by performing the operation A\b. Solve the matrix 3 times once with each of the following DPF values: the ∂A(λ)/∂μa(λ) DPF values, the Scholkmann DPF values and the Dunn DPF values.

e. Repeat steps 2b to 2e until the concentrations for each change in CHGB and S has been calculated with all 3 sets of DPF values.

Experiment 1 Results:

Figure 15: Experiment 1 HbO2 results, showing Scholkmann DPF values lead to the most accurate HbO2 Concentrations

Figure 16: Experiment 1 HbO results, showing Scholkmann DPF values lead to the most accurate HbO Concentrations

Table 12: Absolute difference between the slope and a perfect slope of 1 for experiment 2

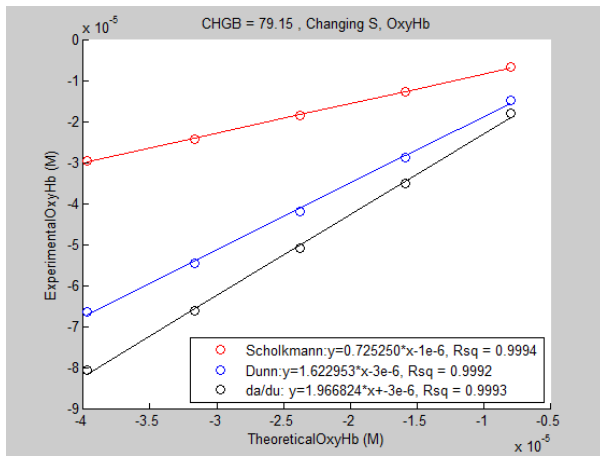|	HbO2	HbO
Scholkmann DPF Absolute Difference	0.275	0.292
Dunn DPF Absolute Difference	0.622	.588
∂A(λ)/∂μa(λ) DPF Absolute Difference	.967	1.265

21

Experiment 2 Results:

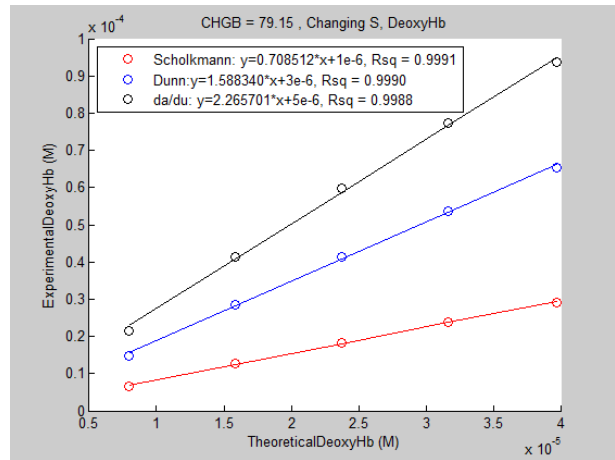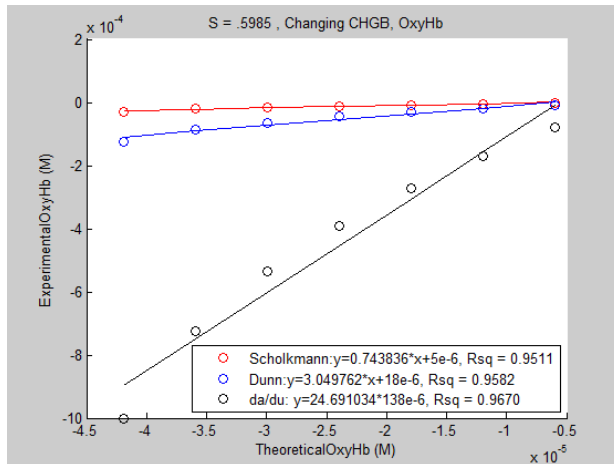Figure 17: Experiment 2 HbO2 Results, showing Scholkmann DPF values lead to the most accurate HbO2 Concentrations
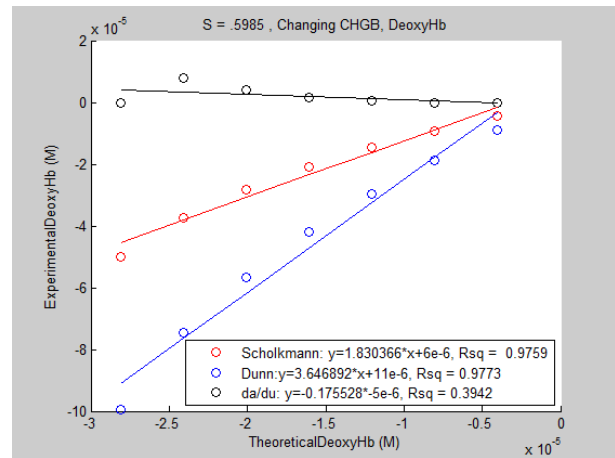
Figure 18: Experiment 2 HbO Results, showing Scholkmann DPF values lead to the most accurate HbO Concentrations

Table 13: Absolute difference between the slope and a perfect slope of 1 for experiment 2

	HbO2	HbO
Scholkmann DPF Absolute Difference	0.256	.830
Dunn DPF Absolute Difference	2.049	2.647
$\partial A(\lambda)/\partial \mu a(\lambda)$ DPF Absolute Difference	23.691	1.175

The results of the experimental relative HbO2 and HbO concentrations for each set of DPF values were plotted against the theoretical relative HbO2 and HbO concentrations. In a graph where the experimental values and theoretical values are plotted against each other, the slope determines how well the experimental values match the theoretical values. The closer the slope is to 1, the closer the experimental values are to the theoretical values. The absolute difference tables show the difference between the slope and a perfect slope of 1. This allowed me to

compare how well each set of DPF values performed. As can be seen by the slopes of the graphs and the absolute difference tables, the experimental relative HbO2 and HbO concentrations were closest to the theoretical relative HbO2 and HbO concentrations when the Scholkmann DPF values were used to solve matrix 1.

The concentration results were the least accurate when using the $\partial A(\lambda)/\partial \mu a(\lambda)$ DPF values and the most accurate when using the Scholkmann DPF values. This may mean the method the Dunn lab group used to calculate their DPF values is superior to the method used in this thesis to calculate the DPF values (also called the $\partial A(\lambda)/\partial \mu a(\lambda)$ DPF values). The Dunn lab group used equation 16 rather than equation 5 to calculate the μ_a values which, were then used to calculate their DPF values. In addition, the CHGB and S values they used to calculate their μ_a were 100 uM and .6 respectively. Whereas, the μ_a values used to calculate the DPF values in this thesis were calculated using equation 5 and the values for CHGB and S were 79.15 uM and .5985 respectively. It was expected that the $\partial A(\lambda)/\partial \mu a(\lambda)$ DPF values would lead to more accurate concentration results since the baseline reflectance values to calculate ΔA, assumed a rat brain would have an initial CHGB of 79.15 and an initial S of .5985 as well. The Scholkmann DPF values had an advantage over the Dunn DPF values since the values 79.15 uM for CHGB and .5985 for S were used to calculate the μ_a values for equation 5.

Both experiments 1 and 2 were modified and performed again with the recalculated Scholkmann DPF values and the $\partial A(\lambda)/\partial \mu a(\lambda)$ DPF values (Table 14 and Table 15). The μ_a values used to calculate the table 14 and table 15 values used values of 100 uM for CHGB and .6 for S. Experiment's 1 and 2 were modified and are listed below as experiments 3 and 4 (the changes made are in red).

Table 14: Scholkmann DPF values calculated with CHGB = 100 uM and S = .6

	560	570	580	590	600	610
Scholkmann DPF Values(Baseline: CHGB = 100 uM, S = .6)	1.3230	1.2479	1.2269	1.8119	2.8594	3.6374

Table 15: $\partial A(\lambda)/\partial\mu a(\lambda)$ DPF values calculated with CHGB = 100 uM and S = .6

	560	570	580	590	600	610
$\partial A(\lambda)/\partial\mu a(\lambda)$ DPF Values(Baseline: CHGB = 100 uM, S = .6)	0.0881	0.0763	0.0747	0.2376	0.7768	1.3755

Experiment 3: Assuming a rat brain has an initial CHGB of 79.15 uM and an oxygen saturation of 59.85%, the initial oxygen saturation was reduced by 10%, 20%, 30%,40%, and 50%. Each time the oxygen saturation was reduced the change in concentration for HbO2 and HbO was calculated by solving matrix 1. Matrix 1 was solved 3 times, once with each set of the DPF values(table 10, 14, 15). After solving for the Hb concentrations, with each set of the DPF values, they were compared to the theoretical Hb concentrations.

Experiment 4: Assuming a rat brain has an initial CHGB of 79.15 uM and an oxygen saturation of 59.85%, the initial total hemoglobin concentration of the tissue was reduced by 10 uM, 20 uM, 30 uM, 40 uM, 50 uM, 60 uM, and 70 uM. Each time the total hemoglobin concentration was reduced, the change in concentration for HbO2 and HbO was calculated by solving matrix 1. Matrix 1 was solved 3 times, once with each set of the DPF values (table 10, 14, 15). After solving for the Hb concentrations, with each set of the DPF values, they were compared to the theoretical Hb concentrations.
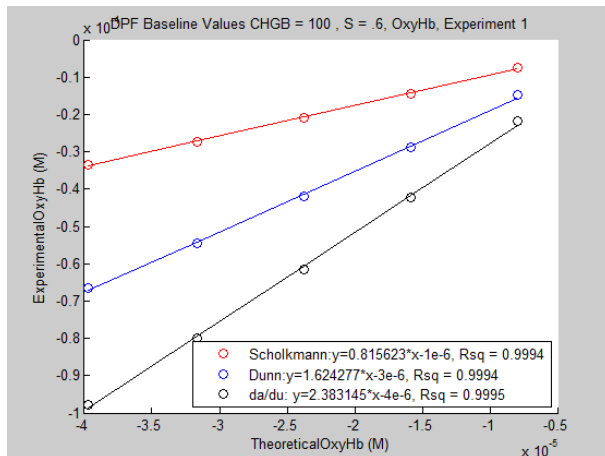
Experiment 3 Results:

Figure 19: Experiment 3 HbO2 Results, showing Scholkmann DPF values lead to the most accurate HbO2 Concentrations

Figure 20: Experiment 3 HbO Results, showing Scholkmann DPF values lead to the most accurate HbO Concentrations

Table 16: Absolute difference between the slope and a perfect slope of 1 for experiment 3

	HbO2	HbO
Scholkmann DPF Absolute Difference	0.184	0.204
Dunn DPF Absolute Difference	0.624	0.589
$\partial A(\lambda)/\partial \mu a(\lambda)$ DPF Absolute Difference	1.383	1.89

Experiment 4 Results:

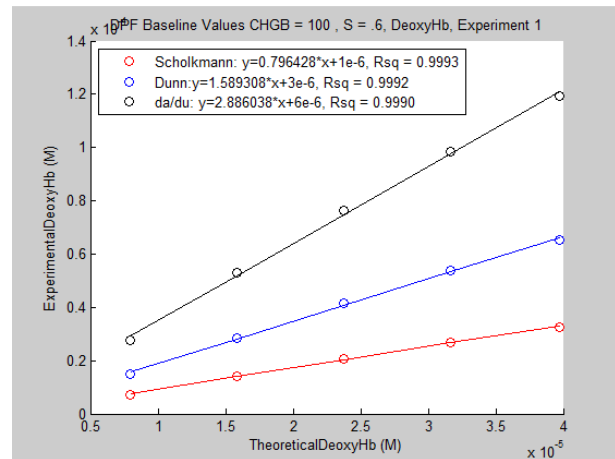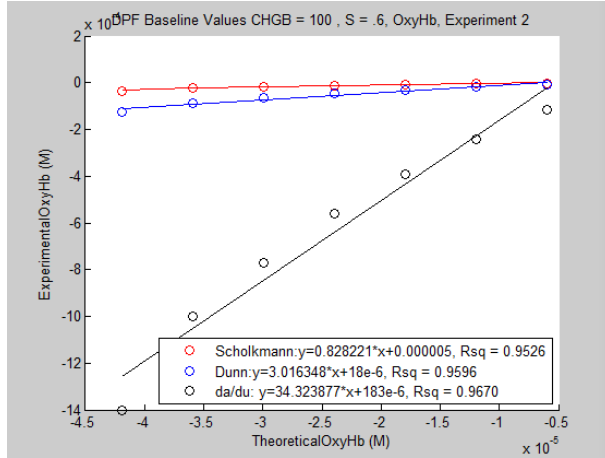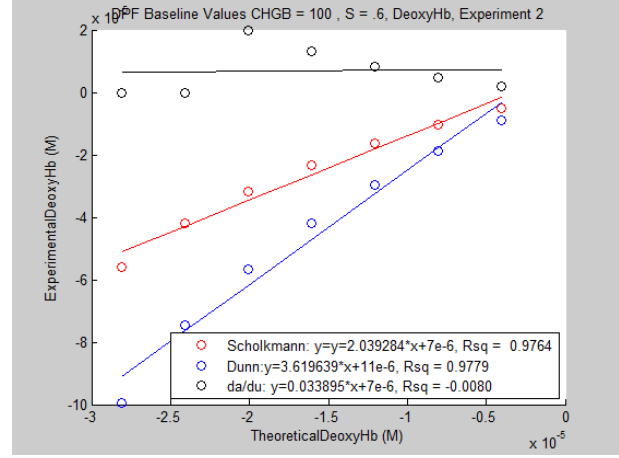Figure 21: Experiment 4 HbO2 Results, showing Scholkmann DPF values lead to the most accurate HbO2 Concentrations

Figure 22: Experiment 4 HbO Results, showing the Da/Dua DPF values lead to the most accurate HbO Concentrations

Table 17: Absolute difference between the slope and a perfect slope of 1 for experiment 4

Scholkmann DPF Absolute Difference	0.172	1.04
Dunn DPF Absolute Difference	2.016	2.62
$\partial A(\lambda)/\partial \mu a(\lambda)$ DPF Absolute Difference	33.324	0.966

The absolute difference results for experiment 3 and 4 show that using the recalculated Scholkmann DPF values (table 14) to solve matrix 1 lead to even more accurate concentration predictions than those made by the old Scholkmann DPF values (table 11) in experiments 1 and 2. In addition, the results for both experiments 3 and 4 of the relative HbO2 and HbO concentrations are more accurate when using the Scholkmann DPF values (table 14) to solve matrix 1 than when using the Dunn DPF values (table 10) and the $\partial A(\lambda)/\partial \mu a(\lambda)$ DPF values (table 15). Thus, the Scholkmann DPF values perform even better when they are calculated with the values 100 uM and .6 for CHGB and S respectively.

I wanted to see how well the old Scholkmann DPF values(table 11) and ∂A(λ)/∂μa(λ) DPF values (table 9) would perform in experiment 1 and 2 compared to the Dunn DPF values (table 10) if the calculated the baseline reflectance values, used to calculate the ΔA values, assumed a rat brain cortex had an initial CHGB of 100 uM and a S of .6. This was done in experiment 5 and 6.

Experiment 5: Assuming a rat brain has an initial CHGB of 100 uM and an oxygen saturation of 60.00%, the initial oxygen saturation was reduced by 10%, 20%, 30%,40%, and 50%. Each time the oxygen saturation was reduced the change in concentration for HbO2 and HbO was calculated by solving matrix 1. Matrix 1 was solved 3 times, once with each set of the DPF values(table 9, 10, 11). After solving for the Hb concentrations, with each set of the DPF values, they were compared to the theoretical Hb concentrations.

Experiment 6: Assuming a rat brain has an initial CHGB of 100 uM and an oxygen saturation of 60.00%, the initial total hemoglobin concentration of the tissue was reduced by 10 uM, 20 uM, 30 uM, 40 uM, 50 uM, 60 uM, and 70 uM. Each time the total hemoglobin concentration was reduced, the change in concentration for HbO2 and HbO was calculated by solving matrix 1. Matrix 1 was solved 3 times, once with each set of the DPF values (table 9,10,11). After solving for the Hb concentrations, with each set of the DPF values, they were compared to the theoretical Hb concentrations.
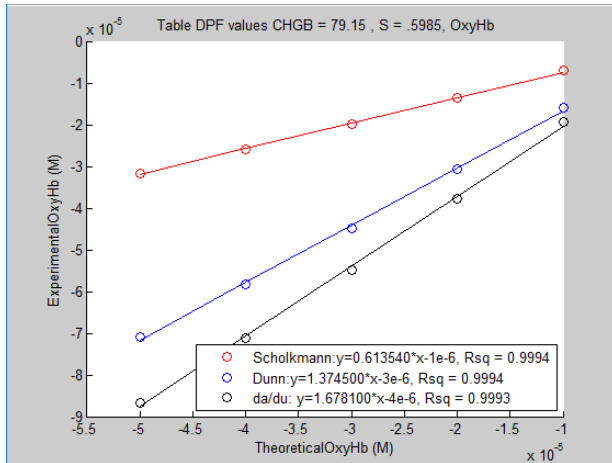
Experiment 5 results:

Figure 23: Experiment 5 HbO2 Results, showing Dunn DPF values lead to the most accurate HbO2 Concentrations

Figure 24: Experiment 5 HbO Results, showing Dunn DPF values lead to the most accurate HbO2 Concentrations

Table 18: Absolute difference between the slope and a perfect slope of 1 for experiment 5

	HbO2	HbO
Scholkmann DPF Absolute Difference	0.386	0.401
Dunn DPF Absolute Difference	0.374	0.346
$\partial A(\lambda)/\partial \mu a(\lambda)$ DPF Absolute Difference	.678	.929

Experiment 6 results:

Figure 25: Experiment 6 HbO2 Results, showing Scholkmann DPF values lead to the most accurate HbO2 Concentrations
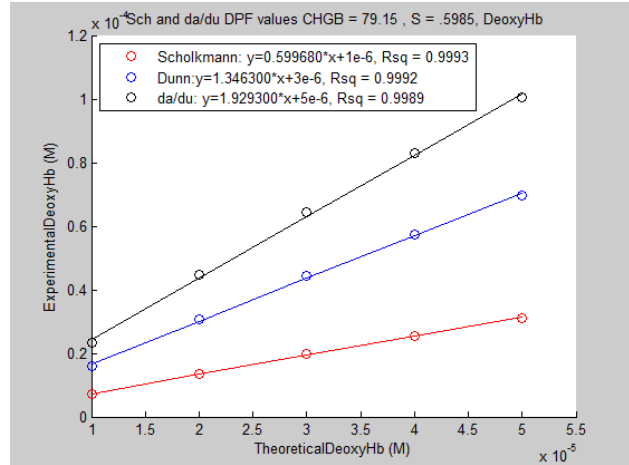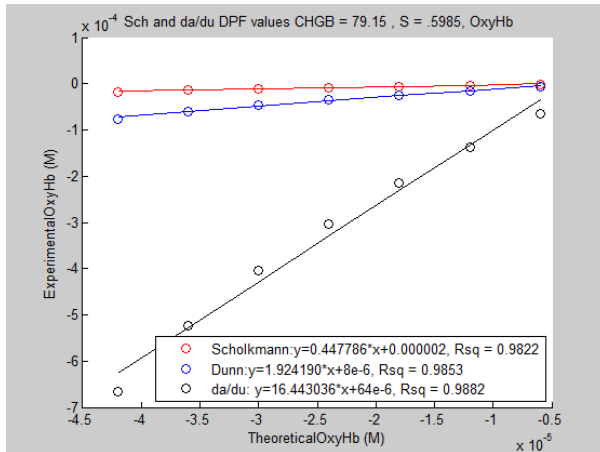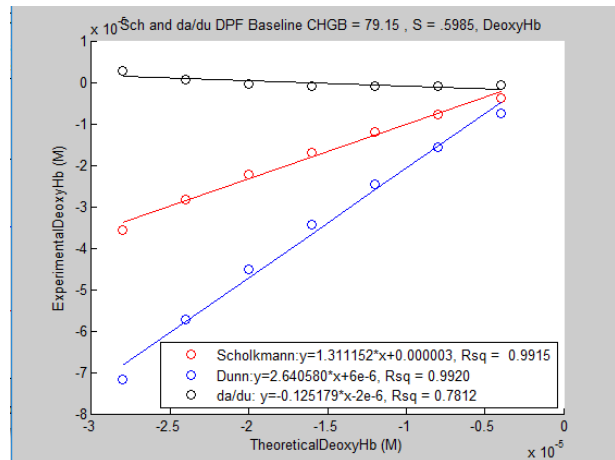

Figure 26: Experiment 6 HbO Results, showing Scholkmann DPF values lead to the most accurate HbO Concentrations

Table 19: Absolute difference between the slope and a perfect slope of 1 for experiment 6

	HbO2	HbO
Scholkmann DPF Absolute Difference	0.553	0.311
Dunn DPF Absolute Difference	0.924	1.641
$\partial A(\lambda)/\partial \mu a(\lambda)$ DPF Absolute Difference	15.4	1.125

It was found that the Dunn DPF values (table 10) when used to solve matrix 1 gave better results than the Scholkmann (table 11) and the $\partial A(\lambda)/\partial \mu a(\lambda)$ DPF values (table 9) for experiment 5. The Scholkmann DPF values (table 11) performed better than the Dunn DPF values (table 10) and the $\partial A(\lambda)/\partial \mu a(\lambda)$ DPF values(table 9) in experiment 6.

The next two experiments test how well the Scholkmann DPF values(table 14) and $\partial A(\lambda)/\partial \mu a(\lambda)$ DPF values (table 15) perform when the ΔA values are found assuming a rat brain cortex has an initial CHGB is 100 uM and .6 for S.

Experiment 5: Assuming a rat brain has an initial CHGB of 100 uM and an oxygen saturation of 60.00%, the initial oxygen saturation was reduced by 10%, 20%, 30%,40%, and 50%. Each time the oxygen saturation was reduced the change in concentration for HbO2 and HbO was calculated by solving matrix 1. Matrix 1 was solved 3 times, once with each set of the DPF values(table10, 14, 15). After solving for the Hb concentrations, with each set of the DPF values, they were compared to the theoretical Hb concentrations.

Experiment 6: Assuming a rat brain has an initial CHGB of 100 uM and an oxygen saturation of 60.00%, the initial total hemoglobin concentration of the tissue was reduced by 10 uM, 20 uM, 30 uM, 40 uM, 50 uM, 60 uM, and 70 uM. Each time the total hemoglobin concentration was reduced, the change in concentration for HbO2 and HbO was calculated by solving matrix 1. Matrix 1 was solved 3 times, once with each set of the DPF values (table 10,14, 15). After solving for the Hb concentrations, with each set of the DPF values, they were compared to the theoretical Hb concentrations.

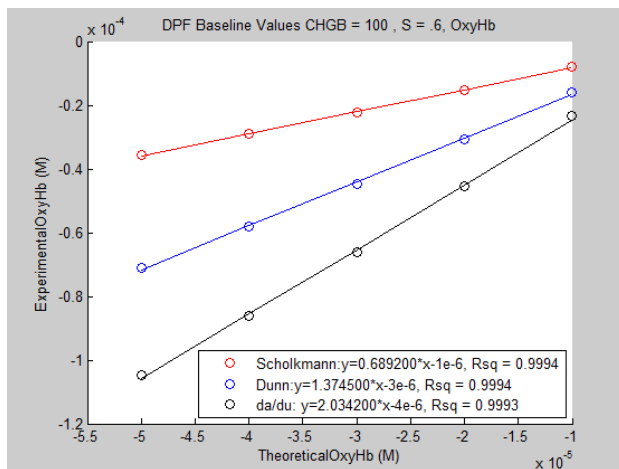Experiment 7 Results:

Figure 27: Experiment 7 HbO2 Results, showing Scholkmann DPF values lead to the most accurate HbO2 Concentrations
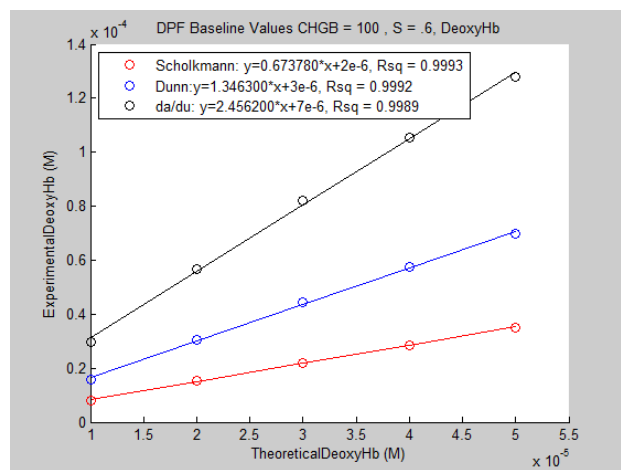
Figure 28: Experiment 7 HbO Results, showing Scholkmann DPF values lead to the most accurate HbO Concentrations

Table 20: Absolute difference between the slope and a perfect slope of 1 for experiment 7

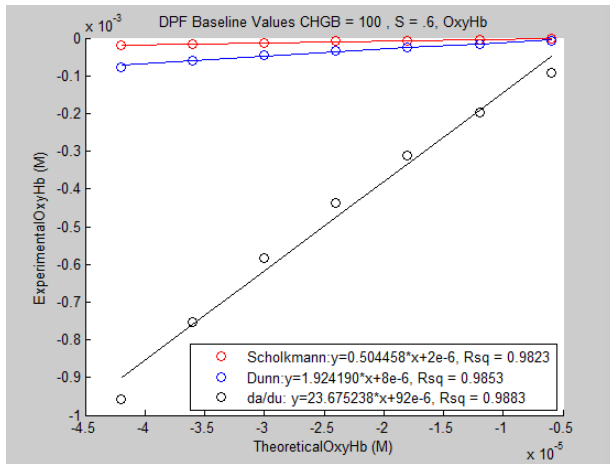|	HbO2	HbO
Scholkmann DPF Absolute Difference	0.311	0.327
Dunn DPF Absolute Difference	0.374	.346
$\partial A(\lambda)/\partial \mu a(\lambda)$ DPF Absolute Difference	1.034	1.46

Experiment 8:

Figure 29: Experiment 8 HbO2 Results, showing Scholkmann DPF values lead to the most accurate HbO2 Concentrations
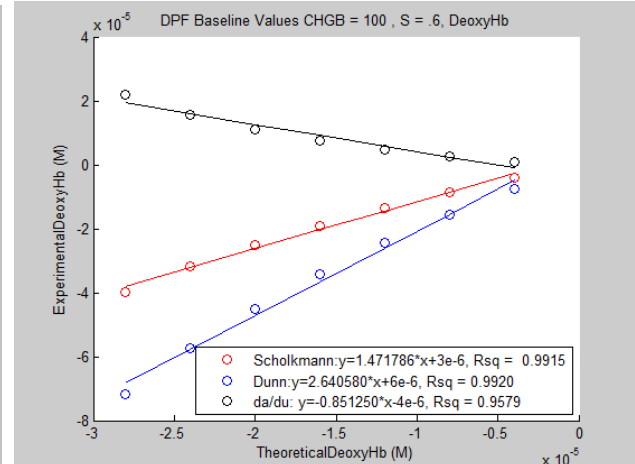
Figure 30: Experiment 8 HbO Results, showing Scholkmann DPF values lead to the most accurate HbO Concentrations

Table 21: Absolute difference between the slope and a perfect slope of 1 for experiment 8

	HbO2	HbO
Scholkmann DPF Absolute Difference	0.496	0.471
Dunn DPF Absolute Difference	0.924	1.641
$\partial A(\lambda)/\partial \mu a(\lambda)$ DPF Absolute Difference	22.68	1.851

It was found in experiment 7 and 8 that the Scholkmann DPF values (table 14) perform better than the $\partial A(\lambda)/\partial \mu a(\lambda)$ DPF values (table 15) and the Dunn DPF values(table 10) when the ΔA values are found assuming a rat brain cortex has an initial CHGB of 100 uM and a S of .6. This can be clearly seen by the experiment 7 and 8 graphs and tables, which illustrate that the slope of the experimental versus theoretical graph is closest to 1 when the concentrations are solved using the Scholkmann DPF values.

3.3 DPF Values Conclusion:

The experiment results show that when the Scholkmann DPF values are used to solve matrix 1, the concentration results are mush closer to the theoretical concentrations compared to the Dunn DPF values and the Scholkmann DPF values in almost every experiment. From experiment 5 and 7 it can be seen the values of CHGB and S, that are used to calculate μ_a values, for the Scholkmann DPF equation can alter the accuracy of the concentration calculations. The first two experiments and the second two experiments show that there is an improvement in the concentrations results when matrix 1 is solved using table 14 rather than table 11. In addition, all experiments show that when the Dunn DPF values are used to solve matrix 1, the concentration results are superior to the $\partial A(\lambda)/\partial \mu a(\lambda)$ DPF values concentration

results. This may mean that the method used to calculate the μ_a values that were used to

calculate the Dunn DPF values may be better than the method used to calculate the μ_a values

for the ∂A(λ)/∂μa(λ) DPF values. Overall, regardless of the values used for CHGB (79.15 uM or

100 uM) and S (.5985 or .6) to calculate the μ_a values and the ΔA values, the Scholkmann DPF

values when used to solve matrix 1 give more accurate relative concentrations for HbO2 and

HbO.

References

1. Emedicine.medscape.com. (2018). *Cerebral Amyloid Angiopathy: Overview, Diagnostic Guidelines, Etiology*. [online] Available at: https://emedicine.medscape.com/article/1162720-overview [Accessed 17 Sep. 2018].

2. Yamada, M., Tsukagoshi, H., Otomo, E. and Hayakawa, M. (1987). Cerebral amyloid angiopathy in the aged. *Journal of Neurology*, 234(6), pp.371-376.

3. Adeoye, Opeolu, and Joseph P. Broderick. "Advances In The Management Of Intracerebral Hemorrhage." *Medscape*. N.p., 2010. Web. 5 Sept. 2018.

4. Foley, A., Ammar, Z., Lee, R. and Mitchell, C. (2015). Systematic Review of the Relationship between Amyloid-β Levels and Measures of Transgenic Mouse Cognitive Deficit in Alzheimer's Disease. *Journal of Alzheimer's Disease*, 44(3), pp.787-795.

5. Dumas, A., Dierksen, G., Gurol, M., Halpin, A., Martinez-Ramirez, S., Schwab, K., Rosand, J., Viswanathan, A., Salat, D., Polimeni, J. and Greenberg, S. (2012). Functional magnetic resonance imaging detection of vascular reactivity in cerebral amyloid angiopathy. *Annals of Neurology*, 72(1), pp.76-81.

6. Hock, C. et al. "Near Infrared Spectroscopy In The Diagnosis Of Alzheimer's Disease.." *Annals of the New York Academy of Sciences* 777.1 (2018): n. pag. Web. 18 Sept. 2018.

7. Ghosh, A. and Osswald, H. (2014). BACE1 (β-secretase) inhibitors for the treatment of Alzheimer's disease. *Chem. Soc. Rev.,* 43(19), pp.6765-6813.

8. Kohl, M., Lindauer, U., Royl, G., Kühl, M., Gold, L., Villringer, A. and Dirnagl, U. (2000). Physical model for the spectroscopic analysis of cortical intrinsic optical signals. *Physics in Medicine and Biology*, 45(12), pp.3749-3764.

9. Scholkmann, F. and Wolf, M. (2013). General equation for the differential pathlength factor of the frontal human head depending on wavelength and age. *Journal of Biomedical Optics*, 18(10), p.105004.

10. StellarNet, Inc. (2018). What is Absorption Spectroscopy? - *StellarNet, Inc.*. [online] Available at: https://www.stellarnet.us/what-is-absorption-spectroscopy/ [Accessed 17 Sep. 2018].

11. Public Lab. (2016). How To Obtain Transmittance/ Absorbance Spectra. [online] Available at: https://publiclab.org/wiki/how-to-obtain-transmittance-absorbance-spectra [Accessed 9 Sep. 2018].

12. Learn.adafruit.com. (2012). Overview | Arduino Lesson 13. DC Motors | Adafruit Learning System. [online] Available at: https://learn.adafruit.com/adafruit-arduino-lesson-13-dc-motors/overview [Accessed 7 Sep. 2018].

13. "Pulse Width Modulation". Electronics Tutorials, 2018, https://www.electronics-tutorials.ws/blog/pulse-width-modulation.html. Accessed 4 Sept 2018.

14. Jacques, Steven L. "Optical Properties Of Biological Tissues: A Review." *Physics in Medicine and Biology* 58.11 (2013): R37-R61. Web.

15. Cuccia, David J. et al. "Quantitation And Mapping Of Tissue Optical Properties Using Modulated Imaging." *Journal of Biomedical Optics* 14.2 (2009): 024012. Web.

16. Dunn, Andrew K. et al. "Spatial Extent Of Oxygen Metabolism And Hemodynamic Changes During Functional Activation Of The Rat Somatosensory Cortex." *NeuroImage* 27.2 (2005): 279-290. Web.